Eur. Phys. J. B **44**, 101–108 (2005)
DOI: 10.1140/epjb/e2005-00104-9

THE EUROPEAN PHYSICAL JOURNAL B

Phase-field simulations for evaporation with convection in liquid-vapor systems

R. Borcia[a] and M. Bestehorn

Lehrstuhl für Theoretische Physik II, Brandenburgische Technische Universität Cottbus, Erich-Weinert-Strasse 1, 03046, Cottbus, Germany

Received 21 May 2004 / Received in final form 24 October 2004
Published online 16 April 2005 –

Abstract. In this paper we propose a phase-field model for analyzing the influence of evaporation on Marangoni convection in liquid-vapor systems. The theoretical description is based on the Navier-Stokes equation with extra terms responsible for describing the Marangoni effect, the heat equation with a supplementary term responsible for describing evaporation phenomena, and the continuity equation. We report on 2D simulations for both Marangoni instabilities in linear approximation and we compare the results with the literature.

PACS. 68.03.Fg Evaporation and condensation – 47.54.+r Pattern selection; pattern formation – 47.20.Dr Surface-tension-driven instability – 05.70.Np Interface and surface thermodynamics

1 Introduction

Phase-field models treat multi-phase systems with complicate interface conditions adequately by tackling the problem continuously, inclusive of the interfacial region. This continuous variation is realized with the help of an order parameter − called phase-field function − which describes the phases thermodynamically. In a classical formulation the basic equations have to be written for each medium and the boundary conditions must be explicitly tracked. In diffuse-interface theory the basic equations − with supplementary terms depending on variations of the phase-field − are written only once for the whole system and interface conditions don't occur.

Proposed for the first time by Langer in an ad hoc manner, the phase-field methodology has recently achieved considerable importance in modeling solidification phenomena [1–5], complex growths structures [6–8] and dynamic fracture [9]. Recently we have extended the phase-field model for describing Marangoni convection (MC) in incompressible layers [10–12], and now we intend to include evaporation in the phase-field simulations on MC.

In this paper we propose a phase-field model for an evaporating fluid heated from below. We are studying a liquid with its own vapor, a situation for which the natural order parameter is the density. For the liquid-vapor system being considered, one assumes the fluids are compressible, with a deformable interface and the evaporating fluid far from criticality (see Fig. 1). The system is bounded in the vertical direction by two rigid and perfectly heat conducting walls with fixed temperatures $T(z = 0) = T_b$ and $T(z = 2) = T_t$ (the length is scaled at the liquid depth d). Due to external heating, both Marangoni instabilities can develop in the liquid-vapor system: the long-wavelength instability induced by surface deflections and the short-wavelength instability driven by a surface tension gradient. A direct application of this model are the experiments performed in microgravity. Consequently, the gravitational force will be ignored in our simulations. The final aim in this paper is to analyze the influence of evaporation phenomenon on both Marangoni instabilities in the frame of the phase-field model.

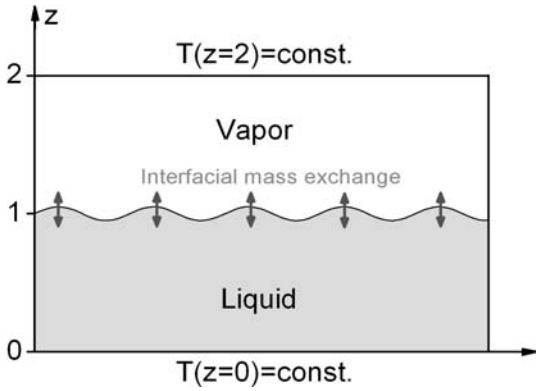

Fig. 1. Sketch of the system under consideration: an evaporating liquid together with its own vapor. The system is heated from below and the temperatures at the top and bottom are maintained constant.

[a] e-mail: borcia@physik.tu-cottbus.de

The paper is organized as follows: Section 2 presents in detail the method adjusted for studying evaporation with convection in liquid-vapor-systems. For realistic fluid parameters, two-dimensional simulations on Marangoni convection (MC) are reported in Section 3. Section 3.1 discusses MC in non-evaporative-systems with compressible fluids. The influence of evaporation parameters on Marangoni instabilities is analyzed in Section 3.2. Finally, principal conclusions are summarized in Section 4.

2 Formulation and basic equations

For the phase-field model in evaporating compressible fluids the appropriate order parameter is the density ρ. For the stationary motionless state the density is assumed to be $\rho_0(z=0)=\rho_l$ at the liquid boundary and $\rho_0(z=2)=\rho_v$ (≈ 0) at the vapor boundary (see Fig. 2). With the help of the density one can continuously express all the other system parameters, respectively, dynamic viscosities, thermal conductivity, heat capacity: $\eta = (\eta_v - \eta_l\frac{\rho_v}{\rho_l})/(1-\frac{\rho_v}{\rho_l}) + (\eta_l-\eta_v)\frac{\rho}{\rho_l}/(1-\frac{\rho_v}{\rho_l})$, $\lambda = (\lambda_v - \lambda_l\frac{\rho_v}{\rho_l})/(1-\frac{\rho_v}{\rho_l}) + (\lambda_l-\lambda_v)\frac{\rho}{\rho_l}/(1-\frac{\rho_v}{\rho_l})$, $\kappa = (\kappa_v - \kappa_l\frac{\rho_v}{\rho_l})/(1-\frac{\rho_v}{\rho_l}) + (\kappa_l-\kappa_v)\frac{\rho}{\rho_l}/(1-\frac{\rho_v}{\rho_l})$, $c = (c_v - c_l\frac{\rho_v}{\rho_l})/(1-\frac{\rho_v}{\rho_l}) + (c_l-c_v)\frac{\rho}{\rho_l}/(1-\frac{\rho_v}{\rho_l})$ (the index "l" describes the liquid parameters at $z=0$ and the index "v" describes the vapor parameters at $z=2$).

Helmoltz free-energy functional is given by [1,2,13]:

$$\mathcal{F}[\rho]=\int_V \mathcal{L}dV, \quad \mathcal{L}=f(\rho,T)+\frac{\mathcal{K}(T)}{2}(\nabla\rho)^2-\mu\rho \quad (1)$$

where $f(\rho,T)$ represents the free-energy density for the homogeneous system (far from the interface), the second term characterizes the interfacial energy and μ is a Lagrange multiplier (the chemical potential). It ensures mass conservation and results from the Euler-Lagrange equation:

$$\mu=\frac{\partial f}{\partial\rho}-\nabla\cdot(\mathcal{K}\nabla\rho). \quad (2)$$

In stationary conditions an interfacial mass exchange does not exist between the two phases, which means the free-energy density can be chosen as a symmetric "double-well" potential

$$f_0(\rho)=\frac{C}{2}\left(\frac{\rho}{\rho_l}-\frac{\rho_v}{\rho_l}\right)^2\left(\frac{\rho}{\rho_l}-1\right)^2 \quad (3)$$

with two local minima: one corresponding to $\rho=\rho_v$ (≈ 0), for the vapor state and the second one to $\rho=\rho_l$, for the bulk in the liquid phase. (In Fig. 3 the density was scaled with the liquid density at bottom boundary ρ_l and consequently the two minima occur on $\rho=0$ and $\rho=1$, respectively.) Plotting now the thermodynamic pressure $p(\rho,T)=\rho\frac{\partial f}{\partial\rho}-f(\rho,T)$ versus unit volume $(1/\rho)$ for the stationary state, one obtains the Van der Waals curve illustrated in Figure 4, which has at the Maxwell construction $p=0$. A difference between the free-energy densities corresponding to the two minima has to appear in the disturbed states in order to allow for evaporative/condensation phenomena at the interface. We model this vertical relative shift of the minima through a supplementary temperature dependant term:

$$f(\rho,T)=f_0(\rho)+r\left(\frac{\rho}{\rho_l}-1\right)(T-T_0(z)), \quad (4)$$

where $T_0(z)$ describes the temperature distribution of the system in stationary conditions and r is a positive constant which will be discussed later. As one can see from Figure 3, for $T=T_0(z)$ the density of the free-energy is symmetrical, no evaporation/condensation phenomena has set in. If small perturbations induce $T>T_0$ the minimum corresponding to the vapor state is diminished. Therefore the system becomes more stable in the gas state than in the liquid state and evaporation sets in. Vice-versa, for $T<T_0$ the free-energy density in the gas becomes larger than the free-energy density in the liquid and the system condenses.

In many previous works $\mathcal{K}$ from the functional (1) is assumed to be constant. But we have previously shown in [10], in order to describe both Marangoni instabilities it is necessary to consider $\mathcal{K}$ dependent on temperature: $\mathcal{K}=\mathcal{K}_0-\mathcal{K}_T T$ ($\mathcal{K}_T>0$). The argument

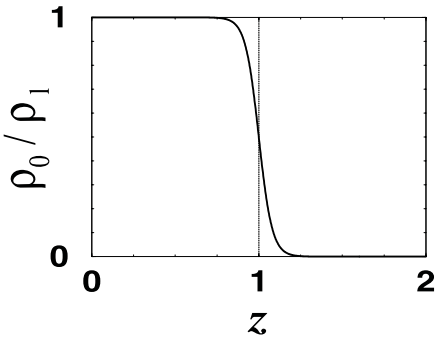

Fig. 2. Density distribution versus z for the stationary state. The diffuse interface between the liquid and the vapor is situated at $z=1$.

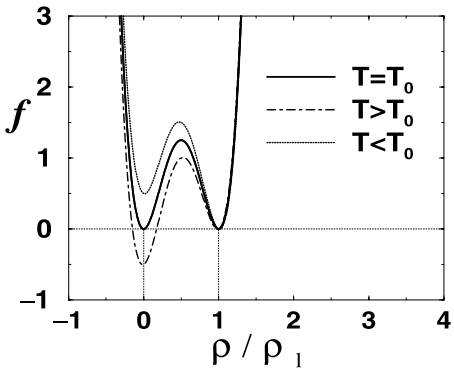

Fig. 3. Free-energy density representation versus density ρ/ρ_l for stationary and perturbated states.

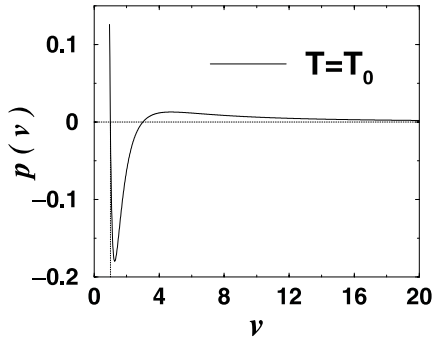

Fig. 4. The pressure curve for stationary state. The unit volumes for liquid and vapor phase correspond to $v_l = 1$ and $v_v = \infty$, respectively.

consists of the fact that $\mathcal{K}$ is connected to the surface-tension coefficient [14,15]

$$\sigma = \int_{-\infty}^{+\infty} \mathcal{K}\left(\frac{\partial \rho_0}{\partial z}\right)^2 dz$$

and the short-wavelength instability is driven by the gradient of the surface tension. Using the Lagrangian formalism (for minimizing the free-energy functional for the equilibrium state), we obtain a new force component in the Navier-Stokes equation [10]:

$$\rho\frac{d\boldsymbol{v}}{dt} = \nabla\mathcal{L} - \nabla\cdot(\mathcal{K}\nabla\rho\otimes\nabla\rho) + \nabla\cdot(\eta\nabla\boldsymbol{v}) + \nabla(\lambda\nabla\cdot\boldsymbol{v}) + \frac{1}{2}\mathcal{K}_T\nabla T(\nabla\rho)^2, \quad (5)$$

where "$\otimes$" denotes the dyadic product and has as components:

$$(\nabla\rho\otimes\nabla\rho)_{ij} = \frac{\partial\rho}{\partial x_i}\frac{\partial\rho}{\partial x_j}.$$

The last term from (5) represents the trigger for short-wavelength instability and assures in the limit of sharp and rigid interfaces the fulfillment of classical interfacial conditions. For incompressible media we have replaced the velocity from (5) with the stream-function

$$\boldsymbol{v} = \frac{\partial\psi}{\partial z}\boldsymbol{i} - \frac{\partial\psi}{\partial x}\boldsymbol{k}.$$

and we have dropped the gradient term $\nabla\mathcal{L}$ applying the curl operator on equation (5) [10–12]. For the model with compressible media developed in this paper there is no stream-function and we need the gradient term $\nabla\mathcal{L}$ in (5). So now one replaces $\mathcal{L} = f(\rho) - \rho\frac{\partial f}{\partial\rho} + \frac{\mathcal{K}(T)}{2}(\nabla\rho)^2 + \rho\nabla\cdot(\mathcal{K}\nabla\rho)$ into (5) leading to a more compact form:

$$\rho\frac{d\boldsymbol{v}}{dt} = -\nabla p + \rho\nabla\left(\nabla\cdot(\mathcal{K}\nabla\rho)\right) + \nabla\cdot(\eta\nabla\boldsymbol{v}) + \nabla(\lambda\nabla\cdot\boldsymbol{v}), \qquad \lambda\approx\frac{\eta}{3}. \quad (6)$$

The above equation coincides with that derived in [14] by Jasnow using an Hamiltonian (canonical) formalism and can also be found in [13] applied there to the problem of film spreading on a solid surface. For the energy equation we consider a supplementary term responsible for describing the latent heat upon evaporative/condensation phenomena [6]

$$\rho c\frac{dT}{dt} = \nabla\cdot(\kappa\nabla T) + L\frac{\partial\rho}{\partial t}, \quad (7)$$

($L-$the latent heat per unit volume (J/kg)). For justifying the last term in (7) one defines the mass flux: $\boldsymbol{J} = \rho\boldsymbol{v}$ which has to satisfy the continuity equation:

$$\frac{\partial\rho}{\partial t} = -\nabla\cdot\boldsymbol{J}.$$

One integrates the equation (7) through the interface in z direction (from liquid to vapor). The integration is performed on a small box enclosing a portion of the interface in such a way that the top of the box is above the surface at height ϵ and the bottom is situated at the same distance below the surface. In the limit of sharp interfaces, taking $\epsilon\to 0$ one can neglect the integral terms which contain the volume forces (for example the integral term which contains the left term from Eq. (7)). Now one introduces in (7) the mass flux $\boldsymbol{J}$ from the continuity equation indicated above. Thus one obtains the boundary conditions which describe the jump of normal heat fluxes [16]

$$\kappa_v\frac{\partial T_v}{\partial z} = \kappa_l\frac{\partial T_l}{\partial z} + LJ_n,$$

where the last term represents the heat flux caused by evaporation.

Summarizing, the fundamental set of equations for MC with evaporation in liquid-vapor systems contains the Navier-Stokes equation (6), the heat equation (7) and the continuity equation for spatiotemporal evolution of the density:

$$\frac{\partial\rho}{\partial t} + \nabla\cdot(\rho\boldsymbol{v}) = 0. \quad (8)$$

3 Numerical results

We scale the variables by using d, d^2/χ_l, χ_l/d, $(T - T_t)/(T_t - T_b)$, ρ_l, η_l, c_l, κ_l as units for the length, time, velocity, temperature, density, viscosity, heat capacity and thermal conductivity where χ represents the thermal diffusivity. The following non-dimensional parameters appear: $P_r = \frac{\eta_l}{\rho_l\chi_l}$ the Prandtl number of the liquid, $Ca = \frac{\sqrt{\mathcal{K}_0 C}\rho_l d}{2\eta_l\chi_l}-$the capillary number, $M = \frac{\mathcal{K}_T\sqrt{\mathcal{K}_0 C}\rho_l}{2\mathcal{K}_0}\frac{(T_t-T_b)d}{\eta_l\chi_l}-$the Marangoni number, $\ell = \frac{\rho_l}{2d}\sqrt{\frac{\mathcal{K}_0}{C}}-$the width of the interface, $E = \frac{L}{c_l(T_t-T_b)}-$the latent heat and $R = \frac{rd^2(T_t-T_b)}{\eta_l\chi_l}-$the bias parameter. We scale the system of equations (6)$-$(8) and we replace the free-energy density from (4) into the pressure term $-\nabla p$ using the thermodynamic relation:

$$p(\rho,T) = \rho\frac{\partial f}{\partial\rho} - f(\rho,T).$$

One becomes now:

$$\frac{\rho}{P_r}\frac{d\boldsymbol{v}}{dt} = -\frac{C_a}{\ell}\rho\nabla[2\rho^3 - 3(1+\rho_v)\rho^2 + (\rho_v^2 + 4\rho_v + 1)\rho - \rho_v(\rho_v+1)] + R\nabla(T-T_0) + \rho\ell\nabla\nabla\cdot[(C_a - MT)\nabla\rho + \nabla\cdot(\eta\nabla\boldsymbol{v}) + \nabla\left(\frac{\eta}{3}\nabla\cdot\boldsymbol{v}\right) \tag{9}$$

$$\rho c\frac{dT}{dt} = \nabla\cdot(\kappa\nabla T) + E\frac{\partial\rho}{\partial t} \tag{10}$$

$$0 = \frac{\partial\rho}{\partial t} + \nabla\cdot(\rho\boldsymbol{v}). \tag{11}$$

There is no evaporation in the stationary state. That means that the density profile $\rho_0(z)$ and the temperature distribution $T_0(z)$, computed numerically from equations (9) and (10), do not depend on E and R. We analyze the linearized system (9)-(11), assuming for the small perturbations plane waves in horizontal direction:

$$\begin{pmatrix}\boldsymbol{v}(x,z,t)\\ T(x,z,t)\\ \rho(x,z,t)\end{pmatrix} = \begin{pmatrix}\boldsymbol{v}_0(z)\\ T_0(z)\\ \rho_0(z)\end{pmatrix} + \begin{pmatrix}\boldsymbol{v}_1(z)\\ T_1(z)\\ \rho_1(z)\end{pmatrix}\exp(ikx+\lambda t) \tag{12}$$

with the wavenumber k (assumed to be real value) and the complex growth-rate λ. This leaves a system of equations depending only on z with derivatives of third order. To solve it we use a finite difference method [17], taking into account the following boundary conditions:

$$v_{x1}|_{z=0} = v_{x1}|_{z=2} = 0, \qquad v_{z1}|_{z=0} = v_{z1}|_{z=2} = 0,$$

$$\rho_1|_{z=0} = \rho_1|_{z=2} = 0, \qquad \left.\frac{\partial\rho_1}{\partial z}\right|_{z=0} = \left.\frac{\partial\rho_1}{\partial z}\right|_{z=2} = 0,$$

$$T_1|_{z=0} = T_1|_{z=2} = 0.$$

In this way the system (9)-(11) is reduced to a linear eigenvalue problem. For the numerical results presented in this section, we have chosen the parameters for a water-vapor system: $P_r = 5.88, \kappa_v/\kappa_l = 0.035, \rho_v/\rho_l = 0.6\times 10^{-3}, \eta_v/\eta_l = 0.013, c_v/c_l = 0.5$, $L = 2.6\times 10^6$ J/kg [18]. The parameter R is proportional to the coefficient r which describes the difference between the free-energy density in the liquid and in the vapor state. That means that r is somehow connected to the energy absorbed/released during evaporation/condensation phenomena and linked to the latent heat L. Assuming the vapor is an ideal gas, one can write for small differences $T-T_0$ a linear dependency between the pressure of the saturated vapor and temperature as follows [16]:

$$p_s(T) = p_0(T_0) + p_T(T-T_0). \tag{13}$$

In the above relation (p_0, T_0) is a point lying on the saturation curve (e.q. $T_0 = 373$ K and $p_0 = 1$ atm for pure water) and the gradient term p_T is given by $p_T/p_0 = L/R_gT_0^2$ ($\approx$0.036 K^{-1} for pure water) with $R_g-$the universal gas constant. Computing now the thermodynamic pressure for the phase-field model one finds: $p(\rho,T) = p_0(\rho)+r(T-T_0)$. So, one can clearly see that r plays the same role as the gradient term p_T from (13). Therefore we have chosen in our simulations for the water-vapor systems $r/C \approx 0.03$ K^{-1}. In Section 3.1 E and R are assumed to vanish, i.e., we analyze the non-evaporative problem in the context of a compressible media. The influence of evaporation on Marangoni instabilities is studied in Section 3.2, where we perform a parametrical study on MC growth rate with respect to E and R.

3.1 Non-evaporative systems

We have started with a very simplified situation for which both fluids are assumed incompressible and the interfacial region perfectly rigid. For this particular situation we don't need the spatiotemporal evolution equation for the density (11) and we consider the variation of ρ_0 given by the analytical solution of equation (9) for the stationary state. Assuming $\rho_v \approx 0$ and $C_a \gg MT$ one obtains:

$$\rho_0(z) = 1/\left[1 + exp\frac{(z-1)}{\ell}\right]. \tag{14}$$

Because the interface is rigid only short-wavelength instability (driven by a surface-tension-gradient) can develop, an instability which appears when the Marangoni number M exceeds a threshold value M_{cr}. For the water-vapor system heated from below we have plotted in Figure 5 the critical Marangoni number M_{cr} and the critical wavenumber k_{cr} versus $1/\ell$. One can observe how for sharp interfaces (namely for large values of $1/\ell$) the results given by the phase-field model converge to the results given by the classical model [16]. The Marangoni number saturates around $M_{cr} \approx 2800$ that means in the terms of the usual definition [19]

$$M' = MB_i/(1+B_i),$$

($B_i = \frac{\kappa_v d_l}{\kappa_l d_v}-$ the Biot number, with $d_l/d_v = 1$) a value $M'_{cr} \approx 95$. The critical wavenumber has its limit at $k_{cr} = 1.98$ (Fig. 5b and inset in Fig. 5a). We note here that the same representations M_{cr} and $k_{cr} = f(1/\ell)$ were presented in our previous work [10] but for a silicon oil-air system heated from below. The same mean result as in the present paper appears: the saturation in the limit of a sharp interface. However, the wavevector at onset is now an increasing function of $1/\ell$ contrary to our earlier result. The slope of the critical wavenumber k_{cr} with $1/\ell$ seems to be strongly connected with the system parameters, especially with the dynamic viscosity ratio, η_{gas}/η_{liq}, which is much larger for the water-vapor system than for the silicon oil-air system.

Now we come back to the model with compressible fluids described by equations (9)−(11). For large values of the capillary number, i.e. for liquid depths above 100 μm, the liquid-vapor interface is quasi-non-deformable and only the short-wavelength instability can occur. For sharp interfaces one obtains $k = 2$ (see Fig. 6a). The stream-lines representation for surface-tension-driven instability together with the density perturbations can be

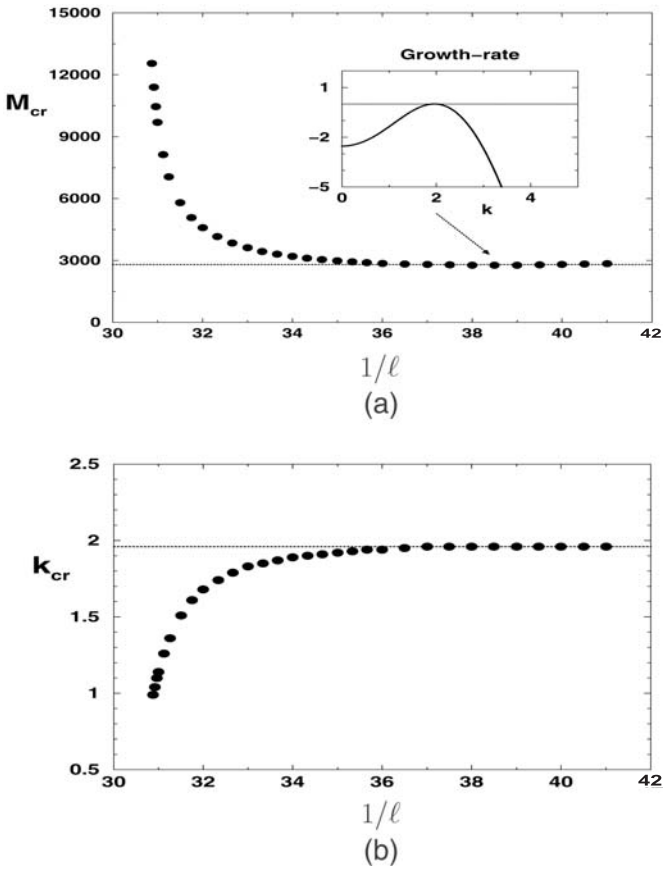

Fig. 5. Dependencies of critical Marangoni number M_{cr} and critical wavenumber k_{cr} on the interface thickness $1/\ell$ for surface-tension-driven instability. The plots follow from the model with incompressible fluids and a perfectly rigid interface.

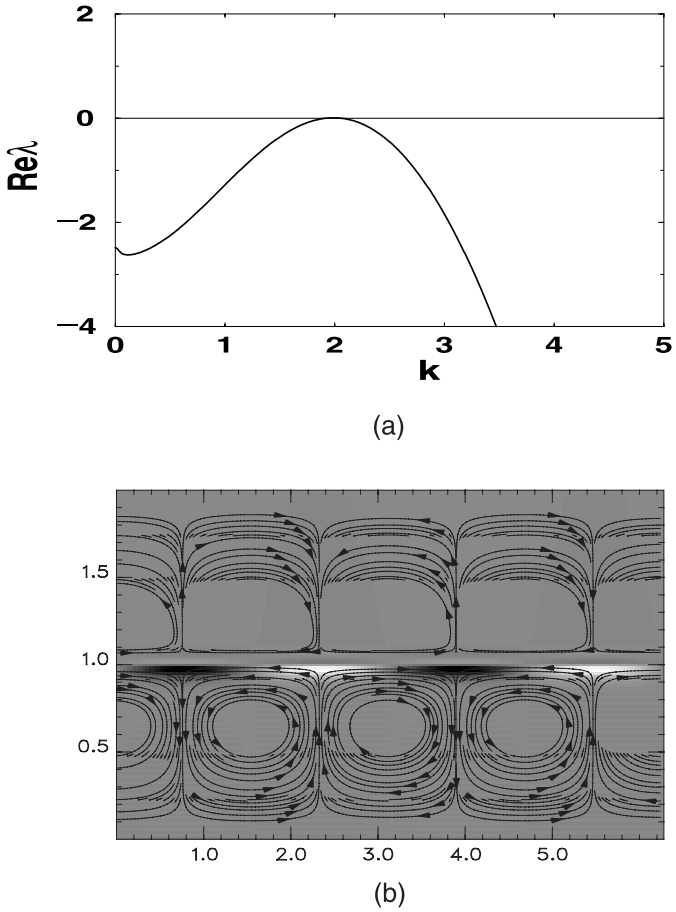

Fig. 6. Growth rate, stream-lines and surface deformations induced by Marangoni instability with short wavelength obtained for the model with compressible fluids and quasi-non-deformable interface ($C_a = 4 \times 10^4$, $\ell = 0.03$, $M = 2820$).

followed in the bidimensional (x, z) representation from Figure 6b. The density perturbations are emphasized in a grey scale, where the grey color means non-perturbated state, the white regions describe the maxima of perturbations and the black regions the minima of perturbations. For compressible fluids there is no stream-function and the stream-lines are computed directly from the velocity components. Figure 6b shows a pattern specific for short-wave instability consisting of two convective motions, one developed in the liquid and the second one in the vapor medium. Respecting density perturbations, Figure 6b shows the location and the width of the interface. More details of the interface deflections can be observed from the 1D representation (versus z direction) illustrated in Figure 7. Here we have plotted the density perturbations caused by the short-wavelength instability in the rising liquid. Convection in liquid pushes the liquid against the interface which leads to an increase of the density at the interface on the liquid side. The advection of vapor from the top plate creates a lower density at the interface. Consequently two peaks appear in (z, ρ_1) representation given by Figure 7, which are asymmetrical because the density in the liquid is larger than the density in the vapor state.

For small capillary numbers (that means for layer depths below 100 μm) the interface becomes deformable

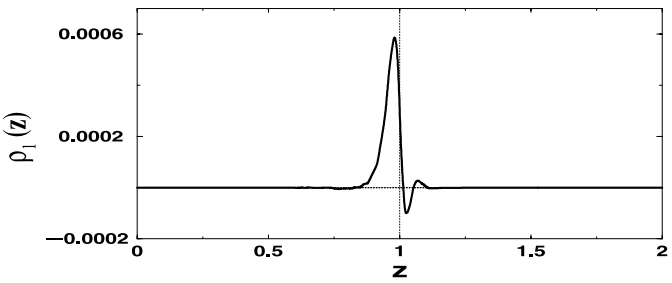

Fig. 7. Density perturbations versus z caused by short-wave instability in a liquid-vapor system with quasi-non-deformable interface. The eigenvalue $\rho_1(z)$ corresponds to the regions where the liquid moves upwards, i.e. for $x = 2.2$ from Figure 6b.

and surface deflections induce convection near $k = 0$ with a long wavelength. In Figure 8a the growth rate for the long-wavelength instability is presented. 2D convection together with the interface deflections are illustrated in Figure 8b. For this kind of instability the pattern consists of large convection rolls developed in almost the whole liquid-vapor system. In the regions where the liquid streams upwards, the convection pushes the lower fluid

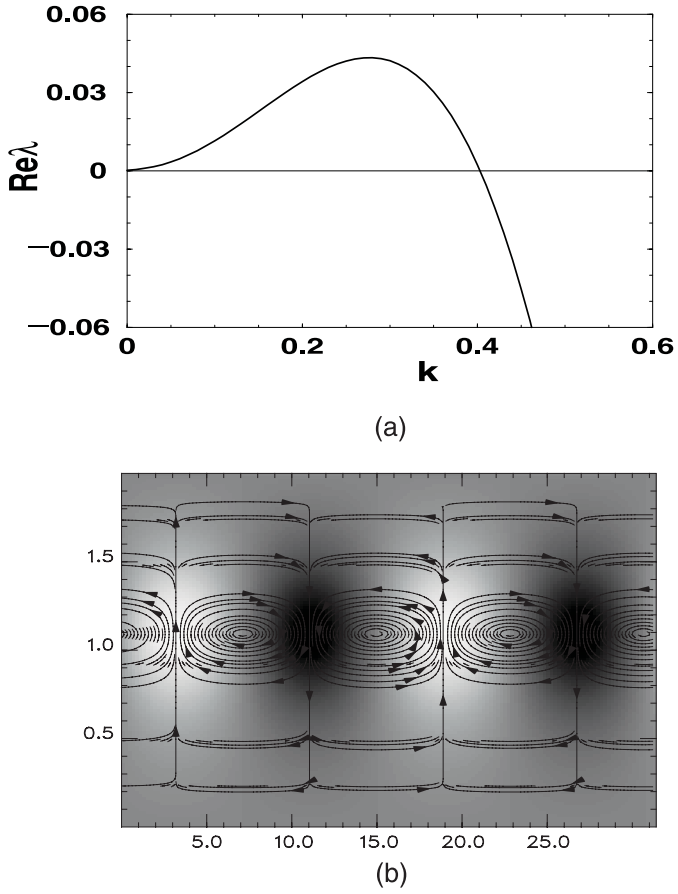

Fig. 8. Growth rate, stream-lines and surface deformations for Marangoni instability with long wavelength. The simulations result from the model with compressible fluids and deformable interface ($C_a = 40$, $\ell = 0.2$, $M = 10$).

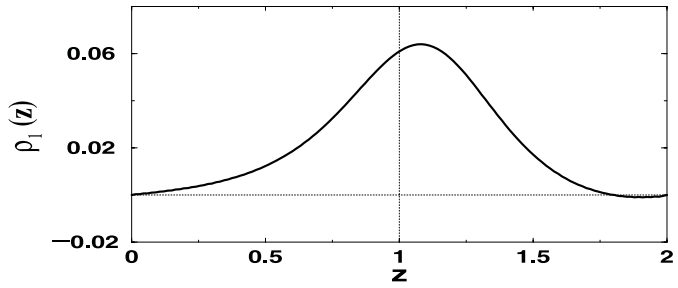

Fig. 9. Density perturbations versus z for long-wave instability developed in a liquid-vapor system with deformable interface. The eigenvalue $\rho_1(z)$ corresponds to regions of a rising fluid, i.e. for $x = 19$ from Figure 8b.

against the interface. Therefore, an increase of fluid density appears around the interfacial region, as observed in Figure 9.

3.2 Evaporation

We shall now investigate the influence of evaporation. To this aim we represent the growth rates for short- and long-wavelength instabilities for different values of E and R. From Figure 10 one can see how evaporation stabilizes the short-wave instability. To explain that we show in Figure 11 the distribution of the temperature perturbation in the z direction along the liquid-gas system corresponding to the regions where the liquid moves upwards, for a single pair of values (E, R). (On the level of linear approximation the temperature perturbation does not seem to depend on E and R). Figure 11 shows a positive temperature perturbation in the whole system inclusive of the interface, outlined by the dotted lines. (The two dotted lines correspond to the values 0.9 and 0.1 of the liquid density, respectively.) As we have already explained in Section 2, a positive temperature perturbation ($(T - T_0) > 0$) causes evaporation at the interface, so the interface is cooled. Analogously, in the regions where the liquid streams downwards condensation occurs and the interface is heated. Consequently the Marangoni effects are diminished. In conclusion, the surface-tension-driven instability is stabilized by the occurrence of evaporation or condensation at the interface.

Evaporation has almost the same effect on long-wavelength instability, as shown in Figure 12. The

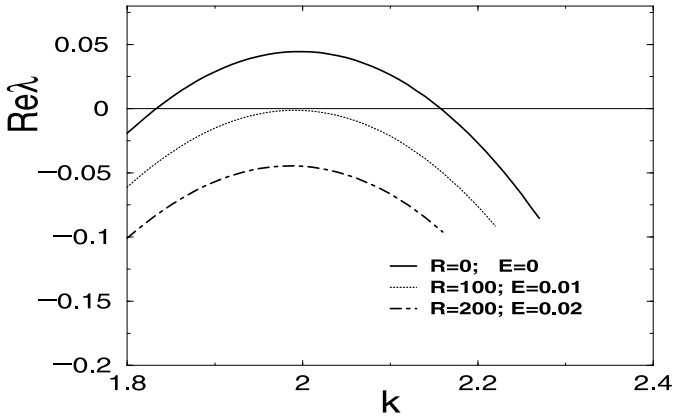

Fig. 10. Growth rates $Re\lambda$ versus wavenumber k for MC with short-wavelength, for different E and R parameters.

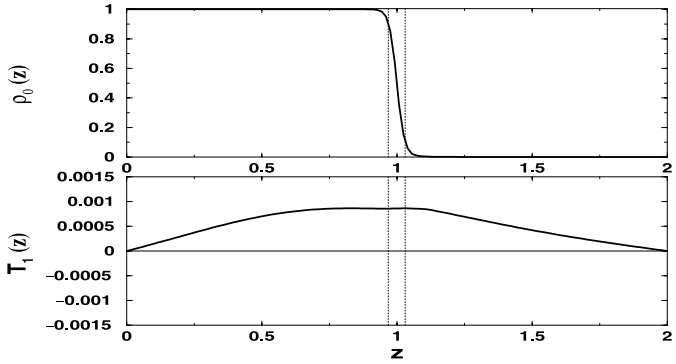

Fig. 11. Interface location and temperature perturbation versus z for a short-wave instability case ($C_a = 4 \times 10^4$, $\ell = 0.03$, $M = 2820$, $R = 50$, $E = 0.005$). The eigenvalue $T_1(z)$ corresponds to the regions where the liquid rises, i.e. for $x = 2.2$ from Figure 6b.

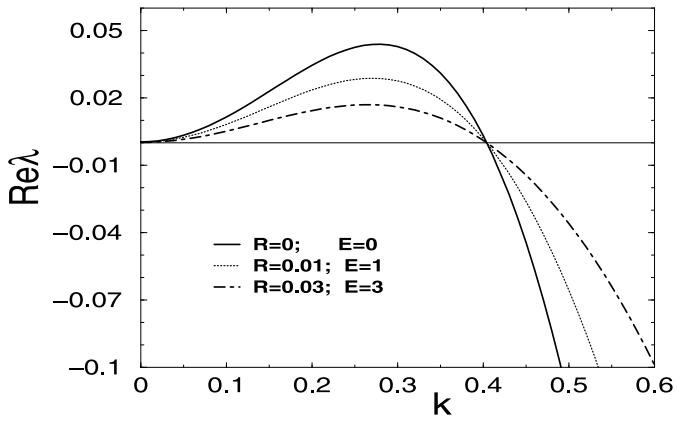

Fig. 12. Same as Figure 10 but for MC with long-wavelength triggered by surface deflections.

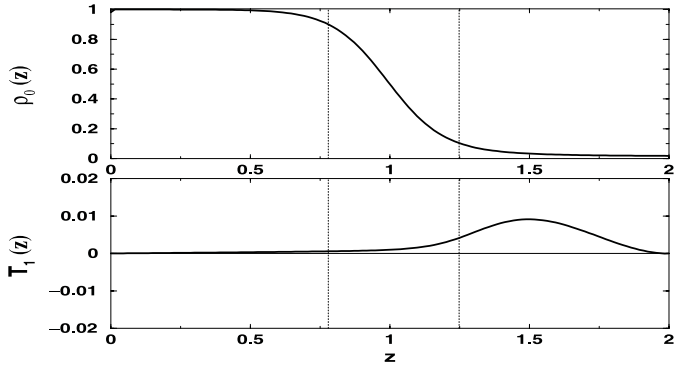

Fig. 13. Same as Figure 11 but for MC with long-wavelength ($C_a = 40$, $\ell = 0.2$, $M = 10$, $R = 0.03$, $E = 3$). The eigenvalue $T_1(z)$ corresponds to regions of a rising fluid, i.e. for $x = 19$ from Figure 8b.

explanation is similar: as in the previous case the temperature perturbation is positive in the rising liquid (Fig. 13). Therefore, evaporation occurs again in the interfacial region which cools the interface and attenuates the convection. However, when the evaporation becomes stronger, the behavior of the curves $\mathrm{Re}\lambda = f(k)$ is different in comparison to the behavior indicated by Figure 10 for short-wave instability. Now the growth-rate is reduced by evaporation but the instability is not really stabilized as in the former case: The instability onset actually rests unchanged, between $k = 0$ and $k = 0.4$ (for the parameters corresponding to Fig. 12). This aspect can be explained going back to equations (9)−(11). The long-wave instability is a so-called type-II_s instability [20] which develops between $k = 0$ and $k = k_1$ (see Fig. 8a). The Marangoni instability with long-wavelength develops in systems with layer depths below 100 μm, a situation for which the interface becomes deformable. For thin layers the bias parameter R becomes very small and does not influence the behavior of the curves $\mathrm{Re}\lambda = f(k)$ represented in Figure 12. The only parameter which plays an essential role in this behavior is the latent heat E. E appears in equation (10) multiplied by the time derivative $\partial\rho/\partial t$. Using the relation (12) one obtains: $E\frac{\partial\rho_1}{\partial t} = E\lambda\rho_1$. At the cut-off point $\lambda = 0$ the term $E\frac{\partial\rho}{\partial t}$ vanishes from equation (10) and consequently k_1 rests unchanged. So k_1 depends in our model on system parameters and temperature difference top-bottom, but k_1 is not influenced by the parameters which describe evaporation. Therefore due to evaporation the long-wavelength instability will slowly grow, but the unstable band $[0,\ k_1]$ will not change. However, one can conclude that, for systems maintained in a temperature gradient without interfacial mass exchange in a stationary state, evaporation has a "stabilizing effect" on both Marangoni instabilities with short and long-wavelengths.

4 Conclusions

In this paper we developed a phase-field model for MC in compressible media with interfacial mass exchange, a problem which can be discussed in a natural way within the framework of diffuse-interface theories. A numerical code for the 2D problem in linear approximation was developed/used, which successfully describes the pattern formation for both Marangoni instabilities.

The effects of evaporation on Marangoni convection depend on the basic conditions. In [21] a volatile fluid with a free rigid surface without external heating and with strong evaporation at the interface is analyzed. For this case, strong evaporation cools the interface with respect to the top and bottom plates and induces surface-tension-driven instability. In contrast with [21] we studied a two-layer system with external heating and without evaporation in the stationary state. For this case the presence of evaporation at the liquid-vapor interface reduces and stabilizes convective motion. In our paper the interface was assumed to be deformable and therefore both types of Marangoni convection can occur. The parametric study shows that evaporation stabilizes short-wavelength instability and retards the long-wavelength instability. The next step would be to include nonlinear effects in the phase-field model and to analyze the spatiotemporal evolution for Marangoni convection with evaporation in the non-linear regime.

This research was supported by the European Union under the network ICOPAC (Interfacial Convection and Phase Change) HPRN-CT-2000-00136.

References

1. J.S. Langer, in *Directions in Condensed Matter*, edited by G. Grinstein, G. Mazenko (World Scinetific, Singapore, 1986), p. 165
2. D.M. Anderson, G.B. McFadden, A.A. Wheeler, Annu. Rev. Fluid Mech. **30**, 139 (1998)

3. D.M. Anderson, G.B. McFadden, A.A. Wheeler, Physica D **135**, 175 (2000)
4. B. Nestler, A.A. Wheeler, L. Ratke, C. Stöcker, Physics D **141**, 133 (2000)
5. L. Ratke, Metallurgical and Material Transactions A **34**, 449 (2003)
6. R.J. Braun, B.T. Murray, J. Cryst. Growth **174**, 41 (1997)
7. X. Tong, C. Beckermann, A. Karma, Q. Li, Phys. Rev. E **63**, 061601 (2001)
8. L. Gránásy, T. Pusztai, J.A. Warren, J.F. Douglas, T. Börzsönyi, V. Ferreiro, Nature Materials **2**, 82 (2003)
9. A. Karma, D.A. Kessler, H. Levine, Phys. Rev. Lett. **87**, 045501 (2001)
10. R. Borcia, M. Bestehorn, Phys. Rev. E **67**, 066307 (2003)
11. R. Borcia, M. Bestehorn, in *Proceedings of the Fifth General Conference of the Balkan Physical Union BPU-5, Vrnjačka Banja, Serbia and Montenegro, August 25-29, 2003*, edited by S. Jokić, I. Milošević, A. Balaž, Z. Nikolić, p. 1219
12. R. Borcia, D. Merkt, M. Bestehorn, Int. J. Bifurcat. Chaos **14**, 4105 (2004)
13. L.M. Pismen, Y. Pomeau, Phys. Rev. E **62**, 2480 (2000)
14. D. Jasnow, J. Viñals, Phys. Fluids **8**, 660 (1996)
15. J.S. Rowlinson, B. Widom, *Molecular Theory of Capillarity* (Clarendon Press, Oxford, 1982) p. 56
16. P. Colinet, J.C. Legros, M.G. Velarde, *Nonlinear Dynamics of Surface-Tension-Driven Instabilities* (Wiley-V. C. H., Berlin, 2001)
17. C. Hirsch, *Numerical Computation of Internal and External Flows*, Vol. 1 (John Wiley, New York, 1988), p. 201
18. J.P. Burelbach, S.G. Bankoff, S.H. Davis, J. Fluid Mech. **195**, 463 (1998)
19. A. Engel, J.B. Swift, Phys. Rev. E **62**, 6540 (2000)
20. M.C. Cross, P.C. Hohenberg, Rev. Mod. Phys. **65**, 851 (1993)
21. D. Merkt, M. Bestehorn, Physica D **185**, 196 (2003)